Electronic Supplementary Material (ESI) for Inorganic Chemistry Frontiers.

Archimedean Heterologous Helix of $Ti_{10}Cd_6$-oxo Nanocluster: Double-Helical Self-Assembly and Therapeutic Application in Parkinson's Disease

Ling-Cui Meng,[a‡] Jun-Yi Chen,[b‡] Zhi-Ming Feng,[a] Zhan-Guo Jiang, [a] * Zhigang Jin [b] * and Cai-Hong Zhan [a] *

a, Key Laboratory of the Ministry of Education for Advanced Catalysis Materials Institute of Physical Chemistry
College of Chemistry and Materials Science, Zhejiang Normal University
Add: No.688, Yingbin Avenue, Jinhua, Zhejiang, China. Zip: 321004
b, College of Life Science, Zhejiang Normal University, Jinhua 321004, China

E-mail: jzg@zjnu.cn; zgkin@zjnu.edu.cn; chzhan@zjnu.cn

‡These authors contributed equally to this work.

Table of Contents

Physical measurement

UV-Vis spectra were measured on an Analytik Jena S600 UV–Visible spectrophotometer. All optical measurements were performed at room temperature. Powder XRD patterns were obtained using a Bruker D8 Advance X-ray diffractometer with (λ (CuKα) = 1.5405 Å) radiation. High resolution mass spectrometry was recorded on an Agilent 6224 (Agilent Technologies, USA) ESI-TOF-MS spectrometer. Fourier Transform Infrared Spectroscopy (FTIR) was recorded on KBr disk using a Nicolet NEXUS 670 spectrometer between 400 and 4000 cm^{-1}. Thermogravimetric Analyses (TGA) was carried out on a TA Instruments STA499 F5 thermobalance with a 100 $mL \cdot min^{-1}$ flow of nitrogen; the temperature was ramped from 20 °C to 800 °C at a rate of 10 $°C \cdot min^{-1}$. Circular dichroism with MOS-500 circular dichroism spectrometer produced by Bio-Logic of France. Test conditions: light source, Xenon lamp; slit width, 2 nm; scanning step size, 2.0 nm/step; initial wavelength, 200 nm; termination wavelength, 600 nm.

Materials and reagents

All starting materials and regents were purchased from commercial suppliers and used without further purification. Salicylic acid, triethylamine and $Ti(O^iPr)_4$ were purchased from Energy Chemical. Anhydrous. $CdCl_2$ (AR) was purchased from Shanghai Aladdin Biochemical Technology Co., Ltd. R/S-hydrobenzoin were purchased from Bide Pharmatech Ltd. And CH_3OH (AR) and CH_3CH_2OH (AR) were purchased from Sinopharm Chemical Reagent Co., Ltd., China.

Synthesis and characterization of structure

The synthesis of $Ti_{10}Cd_6$

A total of 18.3 mg of anhydrous $CdCl_2$ (0.1 mmol), 27.6 mg of salicylic acid (0.2 mmol), and 4 mL of CH_3OH were mixed in a 20 mL glass bottle, and then 31 μL of $Ti(O^iPr)_4$ (0.1 mmol) and 200 μL triethylamine was added. The solution was sonicated for 5 min and then transferred to an oven at 60 °C for 3 days. After cooling, yellow crystals were obtained, washed with EtOH, and then dried at room temperature (yield ~ 60%).

Crystal data and structure refinement

A suitable crystal was mounted in a Hampton cryoloop with Paratone® N oil cryoprotectant. Intensity data collections were carried out at T = 152 K and T = 158 K with a Bruker D8 VENTURE diffractometer equipped with a PHOTON 100 CMOS bidimensional detector using a high brilliance IμS microfocus X-ray Mo Ka monochromatized radiation (λ = 0.71073 Å). With the aid of Olex2, the structure was solved with the ShelXT structure solution program using Intrinsic Phasing and refined with the ShelXL refinement package using Least Squares minimization. Further details about of the crystal structure determinations may be obtained free of charge via the Internet at https://www.ccdc.cam.ac.uk/ CCDC 2325555 (Rac-$Ti_{10}Cd_6$) and 2330372 (R-$Ti_{10}Cd_6$). The absolute configuration of chiral carbon center of R-hydrobenzoin in R-$Ti_{10}Cd_6$ (R = R-hydrobenzoin) isn't modeling due to the limited structure refinement to 1.4 Å resolution.

Table S1. Crystal data and structure refinement for Rac-$Ti_{10}Cd_6$ and R-$Ti_{10}Cd_6$.

Compound	Rac-$Ti_{10}Cd_6$ (2325555)	R-$Ti_{10}Cd_6$ (2330372)
Empirical formula	$C_{72}H_{80}Cd_6Cl_2O_{50}Ti_{10}$	$C_{98}H_{99}Cd_6O_{52}Ti_{10}$
Formula weight	2969.66	3262.17
Temperature/K	152.00	158.00
Crystal system	monoclinic	monoclinic
Space group	$P2_1/c$	$P2_1/n$
a/Å	30.2905(15)	15.526(6)
b/Å	14.7418(8)	35.762(18)
c/Å	29.9729(16)	25.443(12)
α/°	90	90
β/°	117.849(2)	91.997(11)
γ/°	90	90
Volume/Å^3	11833.9(11)	14118(11)
Z	4	4
ρ_{calc}g/cm^3	1.667	1.534
μ/mm^{-1}	1.810	1.489
F(000)	5816.0	6440.0
Crystal size/mm^3	0.02 × 0.015 × 0.01	0.01 × 0.01 × 0.005
Radiation	MoKα (λ = 0.71073)	MoKα (λ = 0.71073)
2Θ range for data collection/°	4.562 to 50.934	4.308 to 29.45
Index ranges	-36 ⩽ h ⩽ 36, -17 ⩽ k ⩽ 16, -35 ⩽ l ⩽ 31	-10 ⩽ h ⩽ 11, -25 ⩽ k ⩽ 25, -18 ⩽ l ⩽ 18
Reflections collected	66304	18152
Independent reflections	20352 [R_{int} = 0.1040, R_{sigma} = 0.1119]	5119 [R_{int} = 0.1886, R_{sigma} = 0.1539]
Data/restraints/parameters	20352/1158/1263	5119/2510/1237
Goodness-of-fit on F^2	1.030	1.083
Final R indexes [I>=2σ (I)]	R_1 = 0.0971, wR_2 = 0.2677	R_1 = 0.1357, wR_2 = 0.3100
Final R indexes [all data]	R_1 = 0.1431, wR_2 = 0.3199	R_1 = 0.1909, wR_2 = 0.3501
Largest diff. peak/hole / e Å^{-3}	2.42/-1.40	1.00/-0.65

Crystal structure analysis

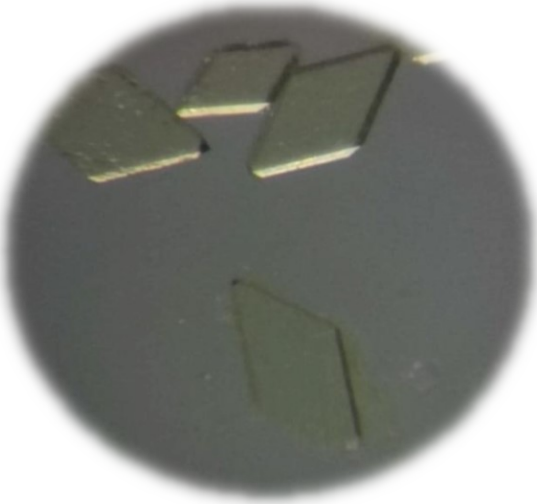

Figure S1. Photograph of Rac-$Ti_{10}Cd_6$ crystals under an optical microscope.

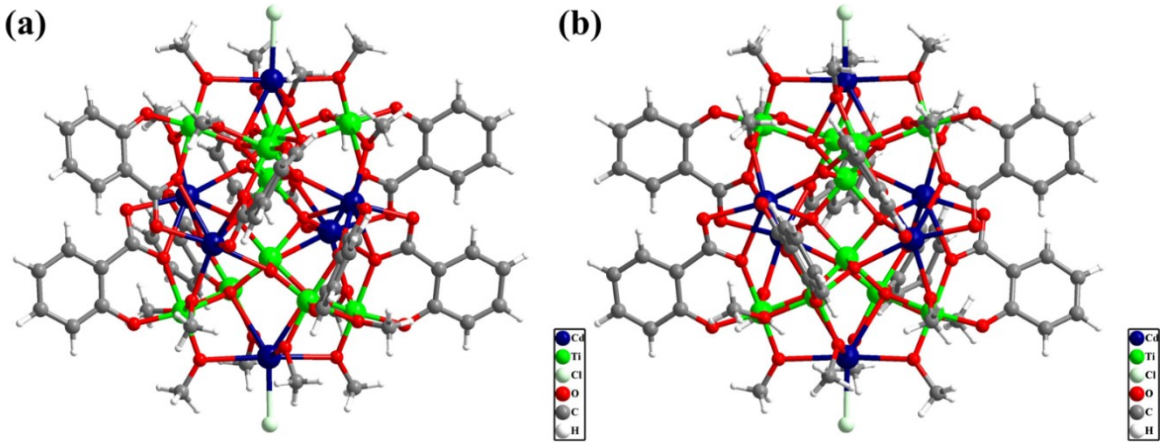

Figure S2. The crystal structures of the *CC* - $Ti_{10}Cd_6$ (a) and *AA* - $Ti_{10}Cd_6$ (b).

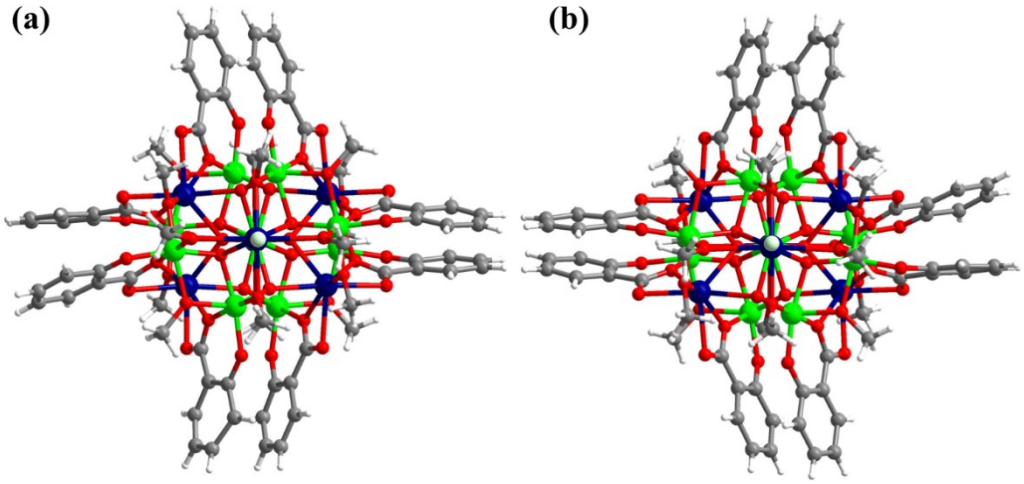

Figure S3. The top views of the *CC* - $Ti_{10}Cd_6$ (a) and *AA* - $Ti_{10}Cd_6$ (b).

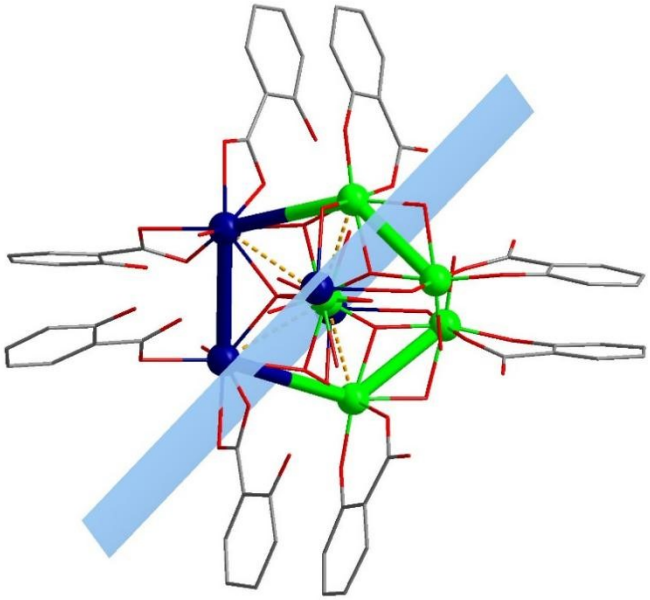

Figure S4. The top view of the diagram of one helix.

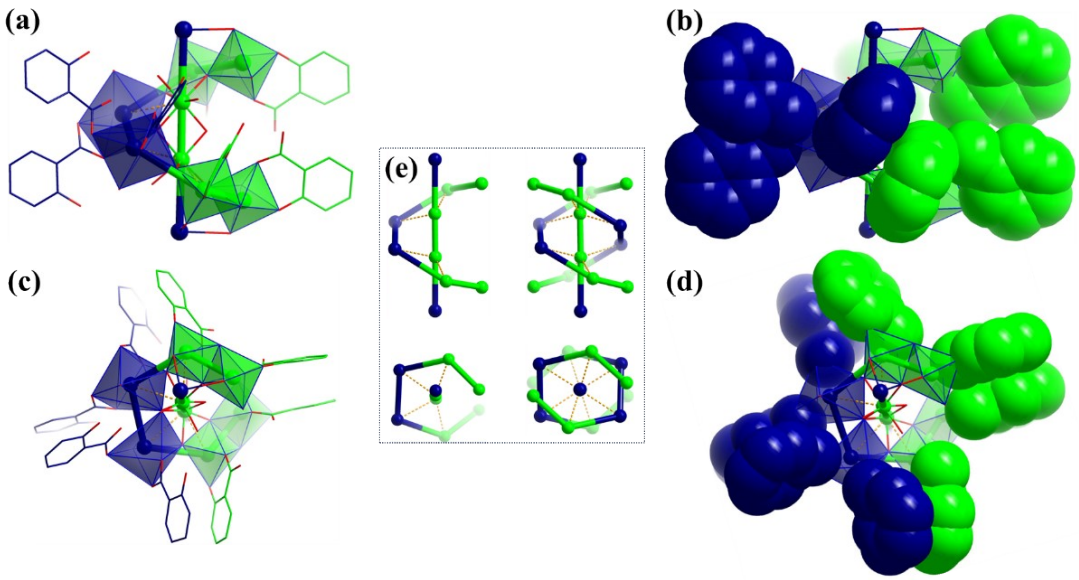

Figure S5. The views of crystal showing one helix in *CC* - $Ti_{10}Cd_6$ (a-d), the side view of polyhedral diagram of different metal ions (a) and space-filling model of ligands (b); the top view of polyhedral diagram of metal ions (c) and space-filling model of ligands (d), for highlighting, ligands that coordinate with metal ions are depicted with the same color as the corresponding metal ions. (e) Ball-and-stick pattern diagrams of metal ion on axis and helix. (Color labels: light green = Ti; dark blue = Cd; red = O, The H atoms are omitted for clarity.)

The two helixes are highlighted in *CC* - $Ti_{10}Cd_6$ as strand A and strand B, and represented in pink and turquoise, respectively (Figure S6a, 6b). The Ti(IV) is coordinated with six O to form an octahedron, while Cd(II) adopts a seven-coordinated polyhedral configuration. Whether it is strand A or strand B, two Ti(IV) octahedra located at the head and tail are connected by edge-sharing, while two Cd(II) polyhedra in the middle adopt corner-sharing mode. Strand A and strand B are wind together through different oxygen atoms of ligands to form the double helixes. As shown in Figure S7, carboxyl oxygen coordinates with Cd(II) on the strand B, while hydroxyl oxygen coordinates with Ti(IV) on the strand A. The Cd(II) and Ti(IV) cations have a shared carboxyl oxygen (Figure S7b, 7c). The pattern is the same for all eight ligands. In order to further understand the relationship between ligands and helixes, we dissected one helix in the *CC* - $Ti_{10}Cd_6$. For clarity, the color of the ligand corresponds to the color of the metal to which it coordinates. Each Ti(IV) octahedron has one ligand and each Cd(II) polyhedron has two ligands. From the top and side view (Figure S5a-S5d), eight ligands can be divided into four groups according to the parallel orientation of the benzene ring, that is the two ligands at the head and tail of the helix, the two ligands in the middle part of the helix and the four ligands coordinate with Ti(IV) octahedron and Cd(II) polyhedron. The four groups ligands, that located at the same height from the side view, are arranged not in the direction of the helix but in a flat along the central axis. The arrangement of the ligand shell can be compared with that of the previous triple-helical structure of the linearly organized $[Au_6Cu_6(4\text{-MeOBT})_{12}]_n$ polymer, in which three external motif follow the the same rotation of three internal kernel.[1]

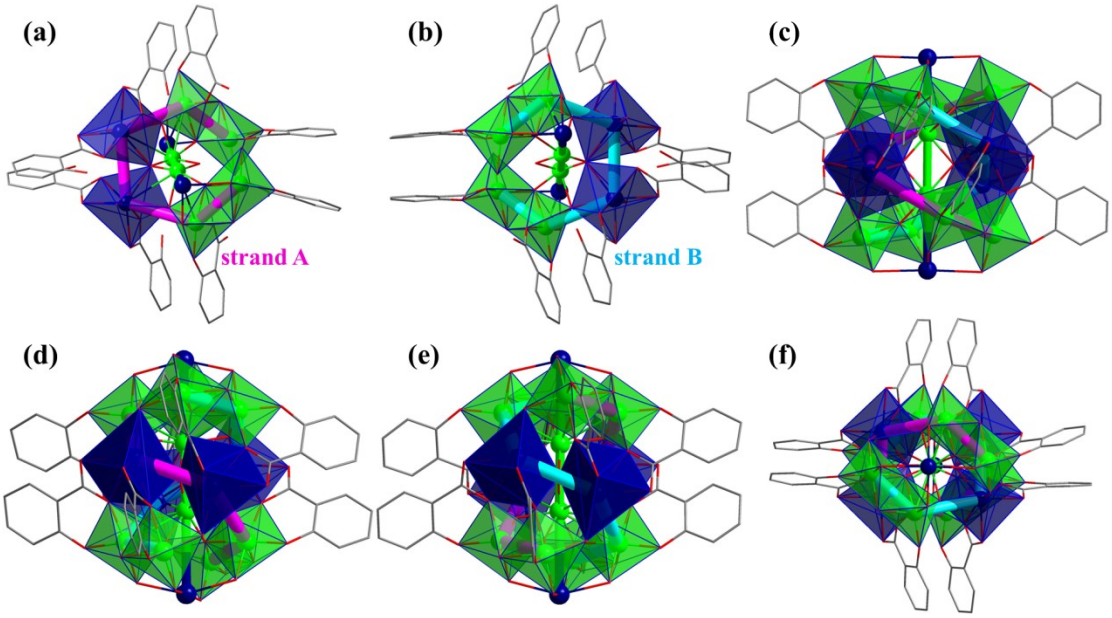

Figure S6. Polyhedral diagrams of metal atoms in strand A (a), strand B (b) and double helixes (c); Coordination environment of Cd(II) polyhedra on strand A (d) and strand B (e); (f) Top view of the polyhedra in double helixes.

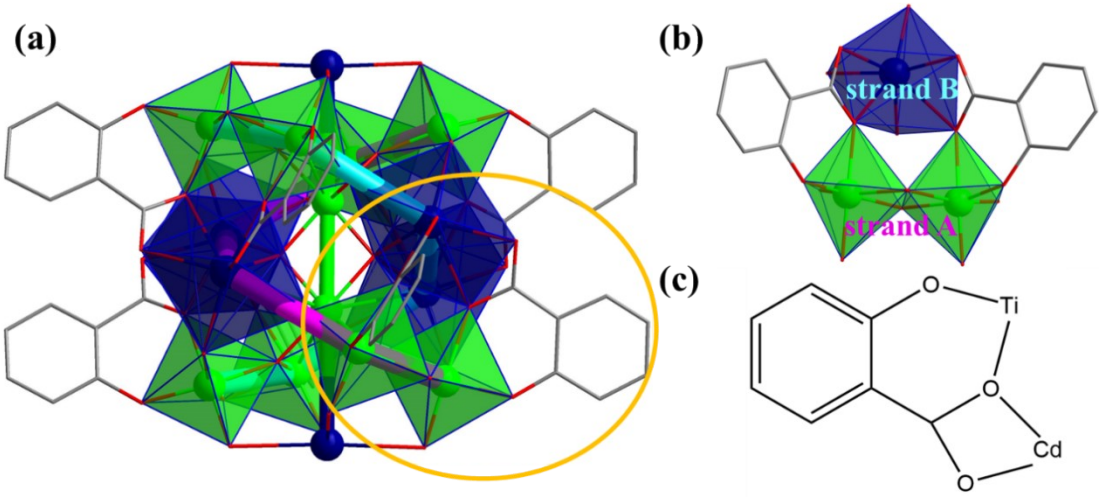

Figure S7. In the *CC* - $Ti_{10}Cd_6$, the two helixes are respectively named strand A (pink) and strand B (turquoise). (a) Polyhedral diagrams of metal atoms in double helixes; (b) the interweaving mode of polyhedra in strand A (pink) and strand B (turquoise) (Highlighted part of the circle in Figure a); (c) Coordination mode of the salicylic acid employed in this work.

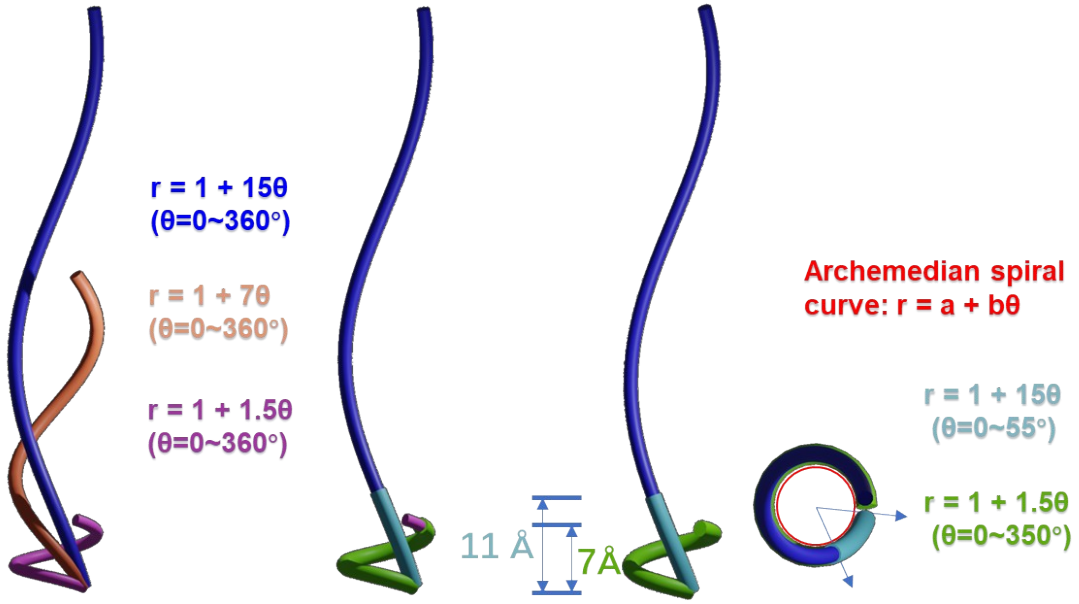

Figure S8. Comparison of Archimedean spiral curves and simulation of single helical structures of Cu_{15} and $Ti_{16}Cd_8$.

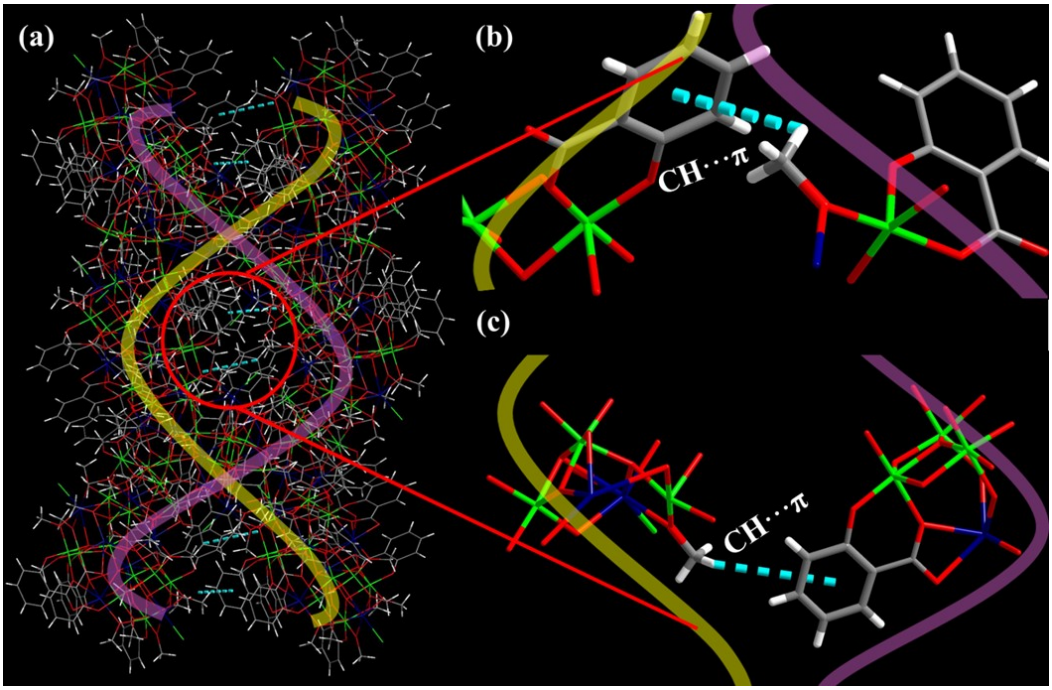

Figure S9. (a) The two helical strands are connected by multiple C-H···π interactions. (b, c) C-H···π contacts are highlighted in turquoise dotted line.

Powder X-ray diffraction (PXRD)

The Powder X-ray diffraction (PXRD) pattern for Rac-$Ti_{10}Cd_6$ can be compared with the simulated pattern obtained from the X-ray single-crystal diffraction analysis. Their peak positions are in good agreement with each other, indicating the phase purity of the products. The differences in intensity may be due to the preferred orientation of the powder samples.

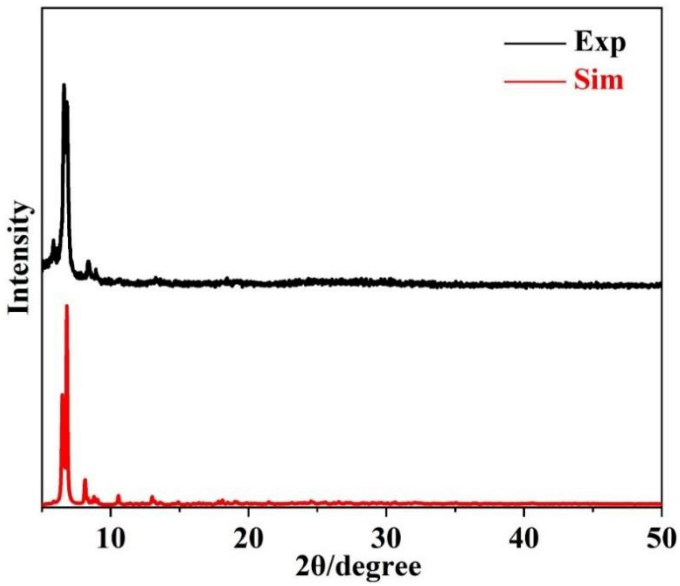

Figure S10. PXRD pattern of Rac-$Ti_{10}Cd_6$.

Fourier transform infrared spectroscopy (FTIR)

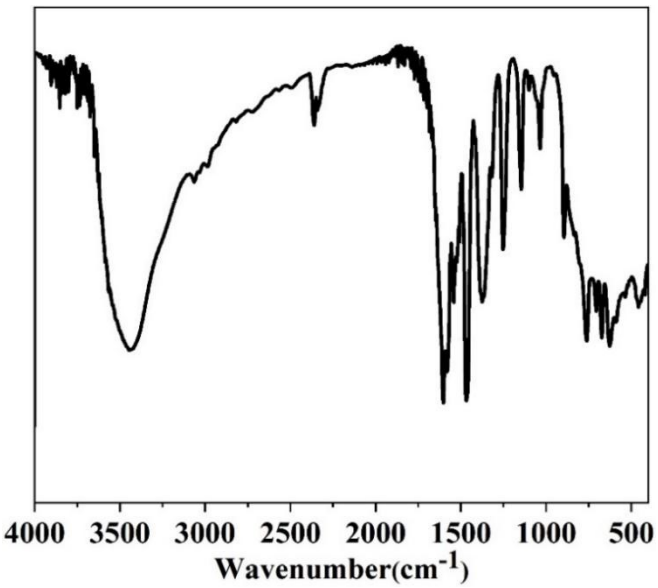

Figure S11. IR spectra of Rac-$Ti_{10}Cd_6$.

Thermogravimetric analyses (TGA)

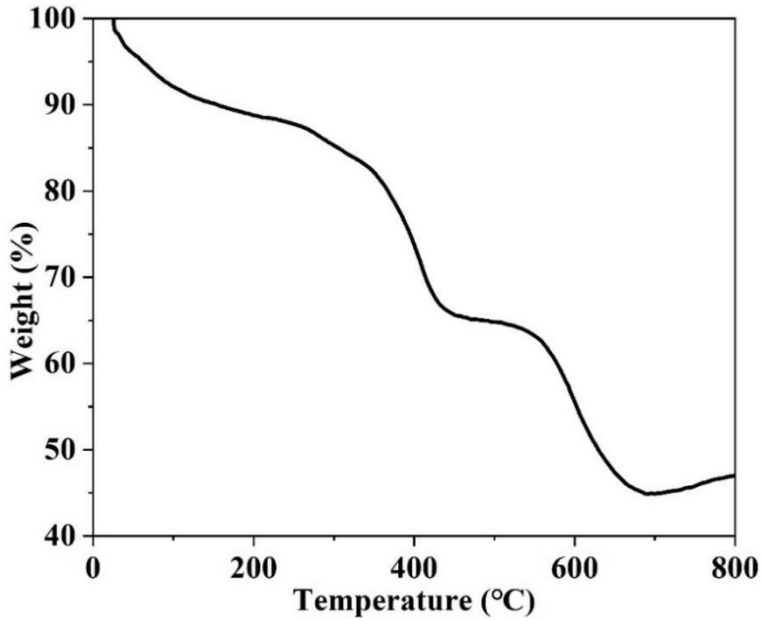

Figure S12. Thermogravimetric analysis trace of Rac-$Ti_{10}Cd_6$.

The thermogravimetric test with heating rate of 10 ºC / min in nitrogen atmosphere shows continuous weight loss from room temperature to 300 ℃, corresponding to the elimination of coordinate solvent molecules, after which the structure begins thermal decomposition.

Deracemization of Rac-$Ti_{10}Cd_6$ solution

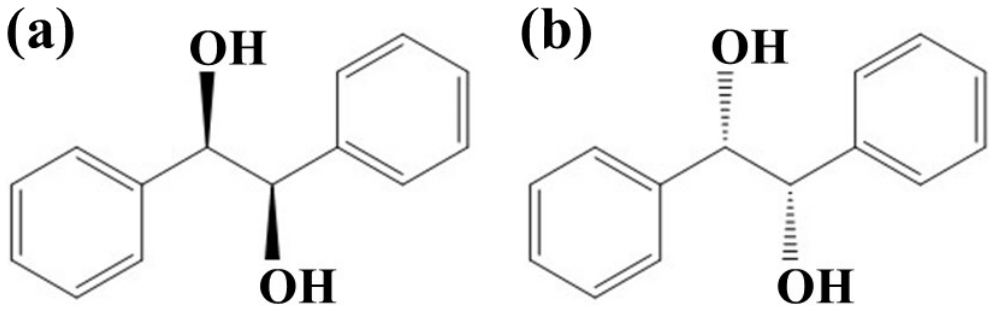

Figure S13. The structures of chiral ligand: R-hydrobenzoin (a) and S-hydrobenzoin (b).

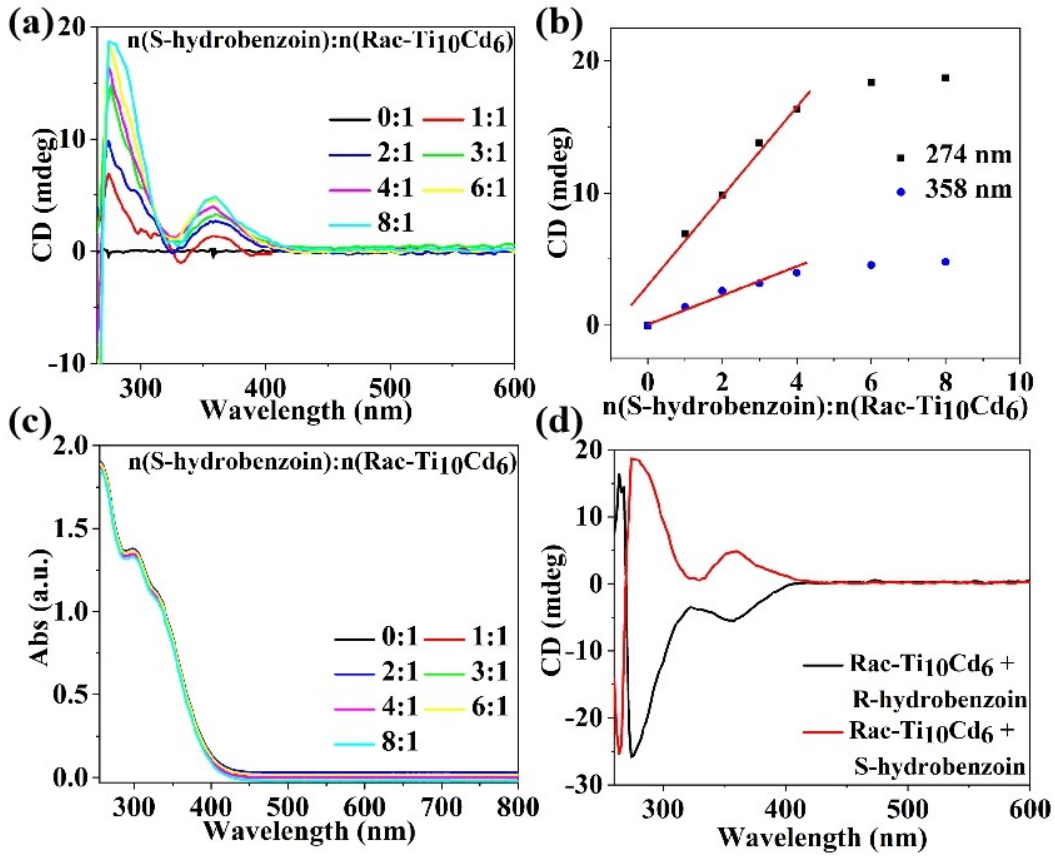

Figure S14. (a) CD titration of Rac-$Ti_{10}Cd_6$ using a chiral ligand (S-hydrobenzoin) in CH_3OH. (b) UV-Vis spectra of Rac-$Ti_{10}Cd_6$ with different amounts of S-hydrobenzoin in CH_3OH. (c) Cotton effects at 274 nm and 358 nm plotted *vs.* the concentration ratio of S-hydrobenzoin and Rac-$Ti_{10}Cd_6$. (d) CD spectra of deracemization of Rac-$Ti_{10}Cd_6$ solution.

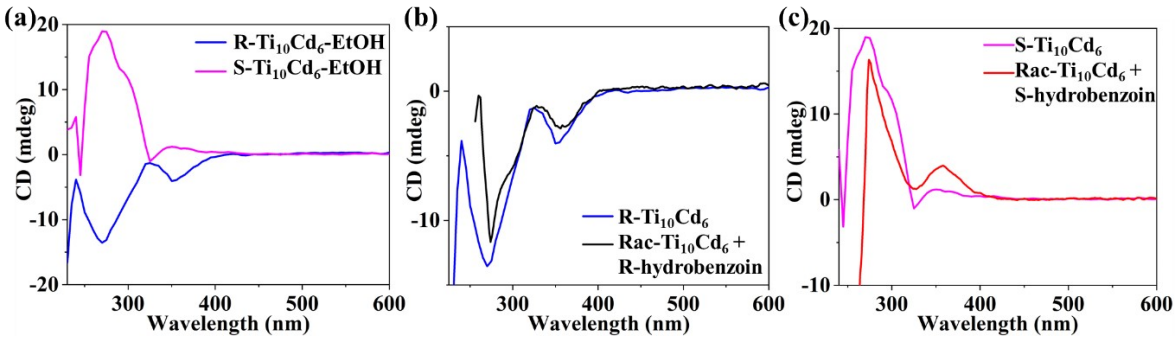

Figure S15. (a) CD spectra of R-$Ti_{10}Cd_6$ (R = R-hydrobenzoin) and S-$Ti_{10}Cd_6$ (S = S-hydrobenzoin) in EtOH solution. (b) Comparison of CD spectra of R-$Ti_{10}Cd_6$ and Rac-$Ti_{10}Cd_6$ + 4 eq (equivalent) R-hydrobenzoin in EtOH solution. (c) Comparison of CD spectra of S-$Ti_{10}Cd_6$ and Rac-$Ti_{10}Cd_6$ + 4 eq S-hydrobenzoin in EtOH solution.

The absolute configuration of chiral carbon center of R-hydrobenzoin in R-$Ti_{10}Cd_6$ (R = R-hydrobenzoin) isn't modeling due to the limited structure refinement to 1.4 Å resolution. As to S-$Ti_{10}Cd_6$ (S = S-hydrobenzoin), ligands shell cannot be totally modeled.

Mass spectrum of R-$Ti_{10}Cd_6$

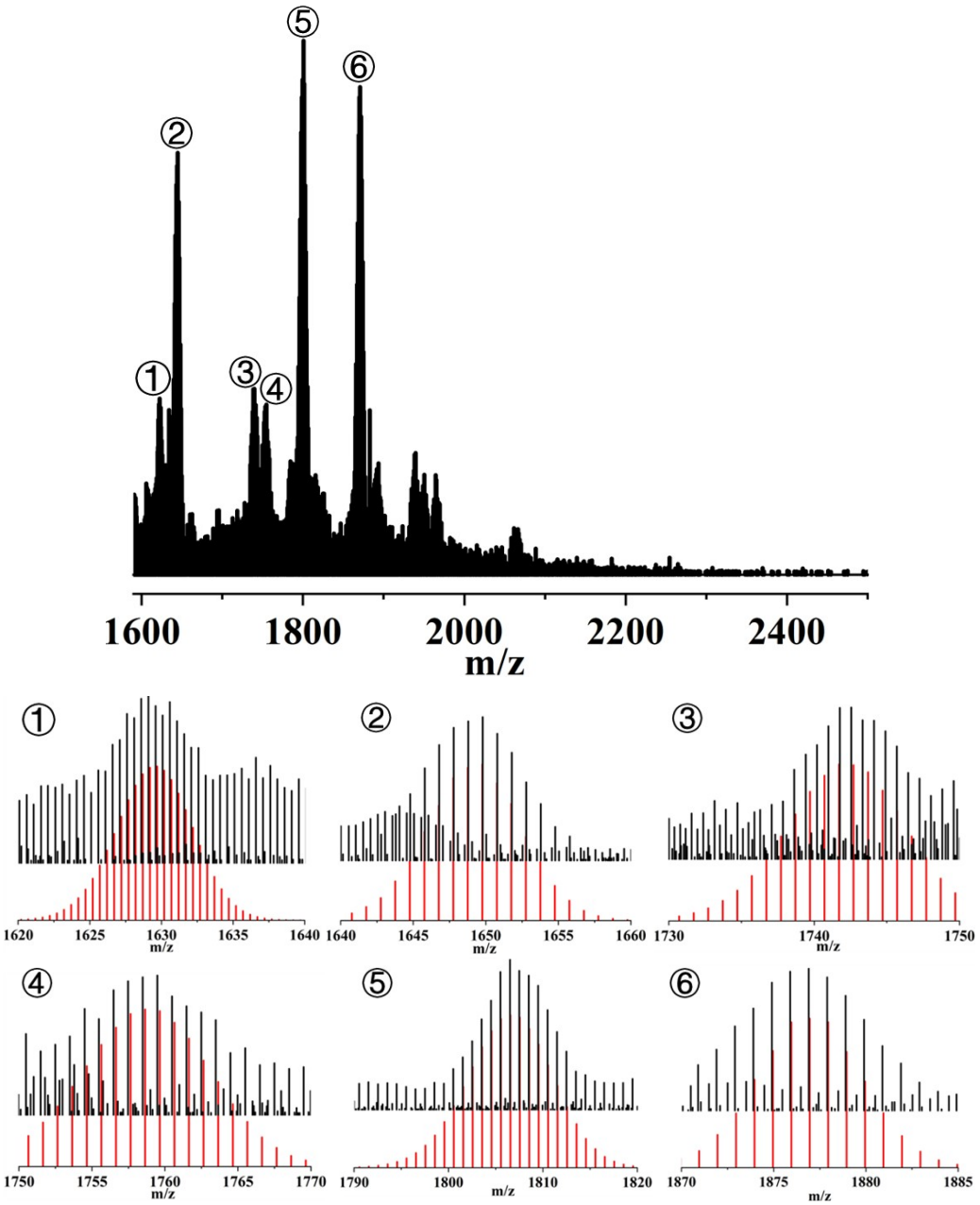

Peak Code	m/z	charge	Envelop Assignment
1	1629.7	-2	$[Ti_{10}Cd_6O_{10}(C_7H_4O_3)_8(OCH_3)_{14}(C_{14}H_{12}O_2)_2]$
2	1649.7	-1	$[Ti_5Cd_2O_4(C_7H_4O_3)_6(OCH_3)_3(C_{14}H_{12}O_2)]$
3	1741.7	-1	$[Ti_4Cd_4O_4(C_7H_4O_3)_4(OCH_3)_7(C_{14}H_{12}O_2) + 2(CH_3OH)]$
4	1758.6	-1	$[Ti_3Cd_5O_3(C_7H_4O_3)_4(OCH_3)_7(C_{14}H_{12}O_2) + (CH_3OH)]$
5	1806.5	-1	$[Ti_4Cd_5O_5(C_7H_4O_3)_4(OCH_3)_7(C_{14}H_{12}O_2)]$
6	1876.9	-1	$[Ti_6Cd_1O_2(C_7H_4O_3)_7(OCH_3)_7(C_{14}H_{12}O_2) + 2(CH_3OH)]$

Figure S16. The ESI-MS spectrum of R-$Ti_{10}Cd_6$ crystals.

Photocatalytic CO_2 reductions activity measurement

Photocatalytic reduction of CO_2 was performed in a 250 mL quartz reactor with as-prepared crystal. Photocatalyst (10 mg) was added into the mixed solution which contains H_2O (38 mL), acetonitrile (4 mL) and triethanolamine (TEOA, 4 mL) as an electron donor. After degassing with high-purity CO_2 to remove dissolved O_2 for 30 min. Light source is the xenon (Xe) lamp (300 W, CEL-HXF300-T3, CHINA EDUCATION AU-LIGHT, China). The reaction temperature was controlled at 303 K by using the cooling water circulation. The gas products analyzed by gas chromatograph (FULI GC9790II gas chromatograph, China) with flame ionization detector.

Mott-Schottky measurement was performed on an electrochemical workstation (CHI 660E, China) in a standard three-electrode cell using a Pt wire and an Ag/AgCl electrode (saturated KCl) as the counter and reference electrodes, respectively. The working electrode was prepared on fluorine-doped tin oxide (FTO) glass with its boundary being protected by Scotch tape. The as-synthesized powder (2 mg) was dispersed into 0.4 mL of C_2H_5OH under sonication for 30 min to obtain a colloidal dispersion. The dispersion was drop-casted onto the FTO glass. After natural air drying, the uncoated part of the FTO glass was isolated with epoxy resin glue. Na_2SO_4 aqueous solution (0.2 M, pH = 6.8) was used as an electrolyte. A solar simulator was utilized as a light source for the measurements.

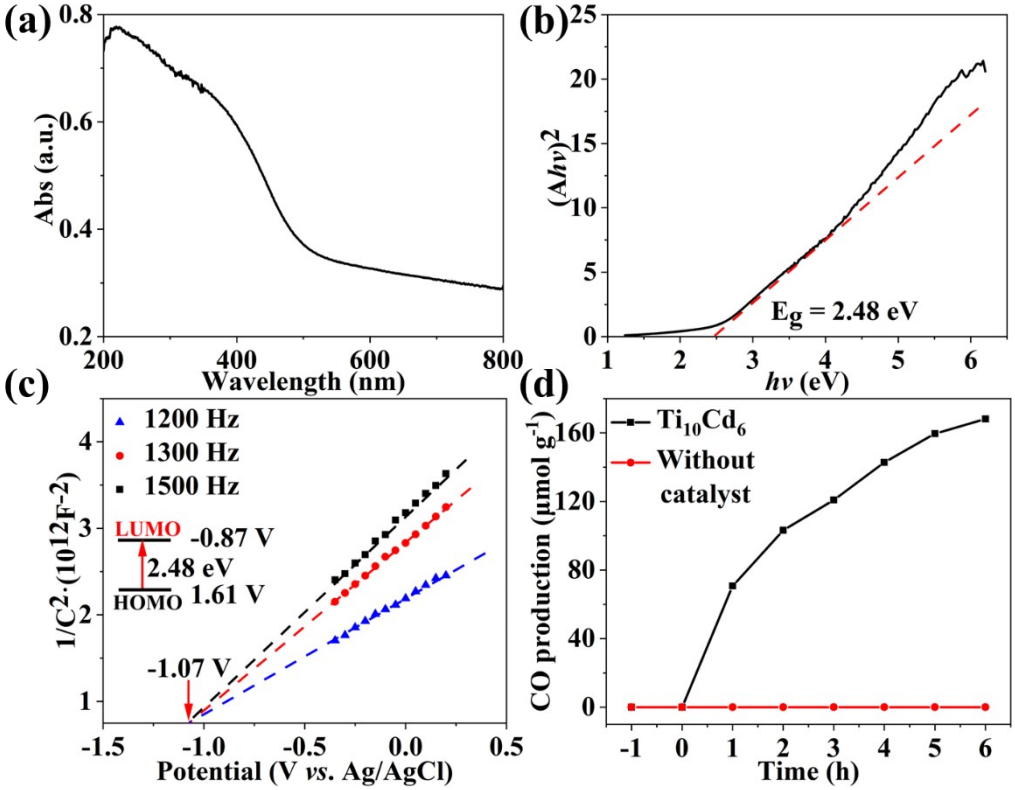

Figure S17. (a) Solid-state UV-Vis diffuse reflectance spectrum of Rac-$Ti_{10}Cd_6$. (b) Tauc plots. (c) Mott-Schottky plots. (d) Time courses of the photocatalytic CO_2 reduction using Rac-$Ti_{10}Cd_6$.

Various Ti-O clusters with differing structures and electronic properties have been characterized in previous studies, primarily focusing on photocatalic water splitting and dye degradation.[2] However, investigations into their application in CO_2 photoreduction remain limited. We conducted CO_2 photoreduction experiments to assess the efficiency of CO_2 reduction catalysis, with all experimental details provided in the supplementary information. The electronic band structure was examined using UV-Vis DRS and Mott-Schottky measurements. Figure S17a illustrates that Rac-$Ti_{10}Cd_6$ exhibits adsorption profiles in the wavenumber range of 200 - 800 nm. The Tauc plot indicates the optical band gap to be 2.48 eV, in line with its yellow color (Figure S17b). Mott-Schottky plots were conducted at three different frequencies (1200 Hz, 1300 Hz, and 1500 Hz) to ascertain the lowest unoccupied molecular orbital (LUMO) energy level, yielding values of -0.87 V *vs.* NHE (Figure S17c). Based on the band gap and Mott-Schottky plot results, the band structure diagram was obtained. The Rac-$Ti_{10}Cd_6$ catalyst demonstrated superior efficacy in CO_2 reduction to CO, attributed to its well-matched band structure and reduction sites. As irradiation time increased, the yields of CO increased simultaneously at different reaction rates. The amount of CO for Rac-$Ti_{10}Cd_6$ reached up to 168.1 μmol g^{-1} after 6 hours (Figure S17d).

The biomedical applications of R/S-$Ti_{10}Cd_6$

Maintenance of *Caenorhabditis. elegans*

C. elegans wild-type strain N2 and transgenic strain UA57 (baIs4, [dat-1p::GFP + dat-1p::CAT-2], GFP expression in dopaminergic neurons) and NL5901 (pkIs2386, [unc-54p::α-synuclein::YFP + unc-119(+)], YFP expression in the muscles) were maintained on nematode growth medium (NGM) agar plates at 20 ℃, which were pre-seeded with *E. coli* OP50 as a food source.[3] Synchronization of *C. elegans* was achieved by treatment with sodium hypochlorite and 5 M NaOH (2:1), which kills adult worms to isolate eggs. The synchronized eggs were cultured in M9 buffer for 24 h till to the first larval (L1) stage for various assays.[4]

Analysis of reproductive and developmental toxicity

To evaluate the potential toxicity of R-$Ti_{10}Cd_6$ and S-$Ti_{10}Cd_6$ on the reproduction in *C.elegans*, the worms N2 at the L1 stage were divided into five groups for treatment with R-$Ti_{10}Cd_6$ or S-$Ti_{10}Cd_6$ (0, 10, 20 μM) till to the L4 stage. Ten L4 worms were selected from each group and each worm was placed in standard NGM agar plate. During the egg-laying period, nematodes were transferred to new plates every 24 h until the loss of reproductive ability. Nematode reproduction was evaluated by brood size. The number of eggs released into the plates each day was counted and the total number of eggs was scored for quantification.

Analysis of developmental toxicity was performed as reported previously.[5] Briefly, worms N2 at synchronized L1 stage were cultivated on standard NGM agar plates for 3 days. Then, L4 worms were transferred to NGM agar plates with various concentrations of R-$Ti_{10}Cd_6$ or S-$Ti_{10}Cd_6$ (0, 10, 20 μM) till adult day 3 and day 6. The adult worms were anaesthetized and mounted in glass slides containing agarose and 5 mM levamisole hydrochloride solution and measured for body length and body breadth with Leica DM4B microsystem.

PD model and measurement of dopaminergic neurons in strain UA57

To establish PD model, 6-OHDA was used to induce dopaminergic neuron degeneration in *C. elegans* as reported previously.[3, 6] The transgenic worms UA57 at synchronized L1 stage were transferred to the NGM and allowed to further develop to the L3 stage. L3 worms were washed twice with sterile water, and exposed to 10 mM

6-OHDA (APExBIO, Shanghai, China) for 2 h under dark condition at 20 ℃ with gentle shake every fifteen minutes. After washing three times with sterile water and centrifuging at 3000 rpm for 1 min, the worms were transferred to NGM agar plates with various concentrations of R-$Ti_{10}Cd_6$ or S-$Ti_{10}Cd_6$ (0, 10, 20 μM) for treatment. 72 h later, the worms were anaesthetized and mounted in glass slides containing agarose and 5 mM levamisole hydrochloride solution (Sangon, Shanghai, China), and imaged for the fluorescence of GFP-labeled dopaminergic neurons with Zeiss LSM880 confocal microscope. Fluorescence intensity of images was analyzed by Image J software to quantify dopaminergic neuron.

Analysis of dopamine-dependent locomotion behaviors

After exposure to 6-OHDA and treatment with R-$Ti_{10}Cd_6$ or S-$Ti_{10}Cd_6$, the worms UA57 were assayed for locomotion behaviors, including body bend, slowing rate and head thrash. For body bend and slowing rate, the worms UA57 were transferred to the fresh NGM agar plates with or without food to adapt for 20 s. After that, the number of body bends of each worm with or without food was separately counted within 20 s with a stereoscopic microscope. The frequency of body bends without food was used for body bend assay. Normally, nematodes crawl more slowly with food than those without food, but disruption of dopamine signaling prevents the nematodes' ability to crawl in the presence of food, thereby enabling faster crawling. Hence, the slowing rate can be calculated as follows: slowing rate = (rate of movement absence of food – rate of movement presence of food) / rate of movement absence of food.[7] For head thrash (the rate of worm movement in liquid), the worms UA57 were dropped in 10 μL M9 buffer and allowed to recover for 20 s.[8] Then, the number of head thrashes within 30 s was counted with a stereoscopic microscope. A head thrash was scored as a head to tail sinusoidal movement.[9] Ten nematodes were scored in each group.

Analysis of α-synuclein aggregation in strain NL5901

The transgenic worms NL5901 at synchronized L1 stage were fed with food OP50 supplemented with R-$Ti_{10}Cd_6$ or S-$Ti_{10}Cd_6$ (0, 10, 20 μM) till adult day 7. Then the worms were anaesthetized and mounted in glass slides containing agarose and 5 mM levamisole hydrochloride solution, and imaged with Zeiss LSM880 confocal microscope. α-synuclein aggregates in head region and body wall muscles were quantified by Image J software. Ten nematodes were scored in each group.

Lifespan

The age-synchronized worms N2 at the L4 stage were transferred to NGM agar plates with various concentrations of R-$Ti_{10}Cd_6$ or S-$Ti_{10}Cd_6$ (0, 10, 20 μM). Three dishes of 30 nematodes per dish were cultured in each group. During lifespan, surviving worms

were transferred to new treatment NGM plates every day. The number of live and dead worms was recorded daily until all the worms in a particular group had expired. The worms would be counted as dead if they did not show any movement when prodded with a platinum wire.

Chemotaxis of N2 *C. elegans* assay

To further confirm that the lifespan effects of R-$Ti_{10}Cd_6$ or S-$Ti_{10}Cd_6$ on nematodes were not caused by dietary restriction, the tropism of avoidance of *C. elegans* was observed. NGM agar plate was equally divided into five groups: DMSO, R-$Ti_{10}Cd_6$ (10 and 20 μM) and S-$Ti_{10}Cd_6$ (10 and 20 μM). Then, 20 μL M9 buffer was dropped at the center of the NGM agar plates, and 50 L4 stage nematodes were picked into M9 buffer. After 2 hours, the number of nematodes on each region was observed and recorded under a stereoscopic microscope. Three NGM agar plates were scored in each group.

Statistical analysis

All values were expressed as mean ± S.E.M. Differences were analyzed by one-way analysis of variance with Dunnett's tests by GraphPad Prism 8.0 software. $P > 0.05$ was considered not statistically significant, and $P < 0.05$ was considered statistically significant (* $P < 0.05$, ** $P < 0.01$, and *** $P < 0.001$).

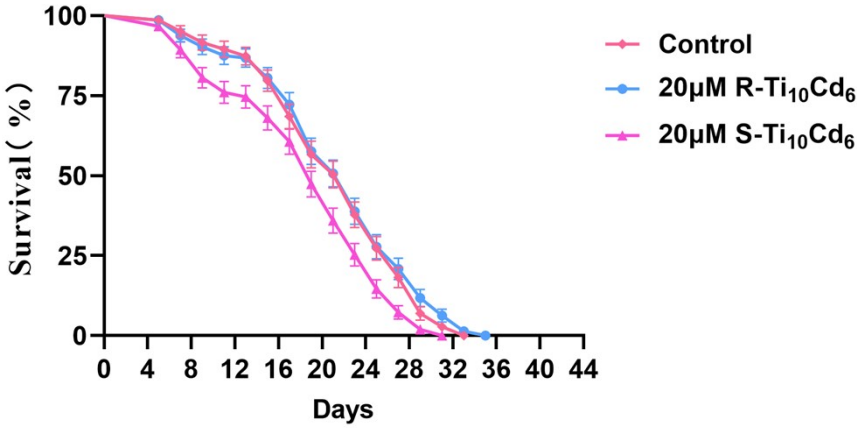

Figure S18. Lifespan experiment of N2 *C. elegans* fed OP50 containing DMSO, 20 μM R-$Ti_{10}Cd_6$ or 20 μM S-$Ti_{10}Cd_6$. All data were expressed as mean ± S.E.M. Statistics: Dunnett's tests (** $p < 0.01$, *vs* the control group).

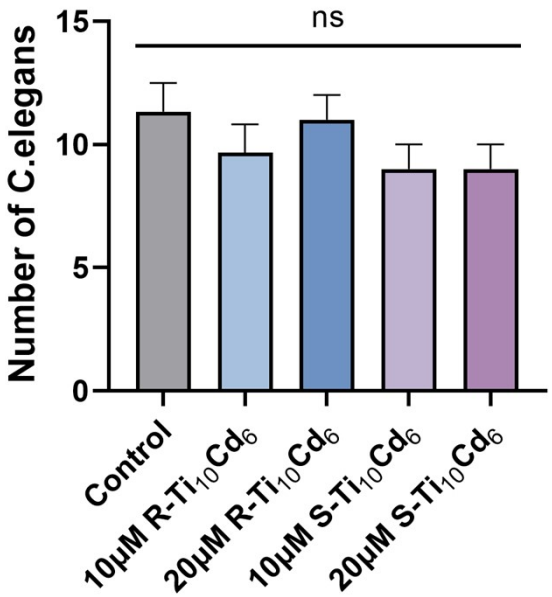

Figure S19. Chemotaxis of N2 *C. elegans* to DMSO, R-$Ti_{10}Cd_6$ (10 and 20 μM) and S-$Ti_{10}Cd_6$ (10 and 20 μM). Statistical analysis indicates no obvious differences between R-$Ti_{10}Cd_6$ or S-$Ti_{10}Cd_6$ treated groups and the control group ($p \geqslant 0.05$).

Reference

[1] H. Li, P. Wang, C. Zhu, W. Zhang, M. Zhou, S. Zhang, C. F. Zhang, Y. P. Yun, X. Kang, Y. Pei, M. Z. Zhu, Triple-helical self-assembly of atomically precise nanoclusters. *J. Am. Chem. Soc.* **2022**, 144, 23205.

[2] a) N. Li, J. Liu, J. J. Liu, L. Z. Dong, S. L. Li, B. X. Dong, Y. H. Kan, Y. Q. Lan, Self-assembly of a phosphate-centered polyoxo-titanium cluster: Discovery of the heteroatom keggin family. *Angew. Chem. Int. Ed.* **2019**, 58, 17260; b) K. Sheng, X. Q. Huang, R. Wang, W. Z. Wang, Z. Y. Gao, C. H. Tung, D. Sun, Decagram-scale synthesis of heterometallic Ag/Ti cluster as sustainable catalyst for selective oxidation of sulfides. *J. Catal.* **2023**, 417, 185; c) L. C. Meng, Z. M. Feng, Z. G. Jiang, C. H. Zhan, A surface-dynamic approach toward supercrystal engineering of titanium-oxo clusters. *Inorg. Chem. Front.* **2023**, 10, 5694; d) K. Z. Su, M. Y. Wu, Y. X. Tan, W. J. Wang, D. Q. Yuan, M. C. Hong, A monomeric bowl-like pyrogallol[4]arene Ti_{12} coordination complex. *Chem. Commun.* **2017**, 53, 9598.

[3] H. L. Li, Y. R. Feng, Z. Y. Chen, X. Jiang, Z. Y. Zhou, J. F. Yuan, F. Li, Y. Zhang, X. X. Huang, S. J. Fan, X. J. Wu, C. Huang, Pepper component 7-ethoxy-4-methylcoumarin, a novel dopamine D2 receptor agonist, ameliorates experimental parkinson's disease in mice and caenorhabditis elegans. *Pharmacol. Res.* **2021**, 163, 105220.

[4] C. J. Ma, Y. Feng, X. Li, L. Sun, Z. He, J. Gan, M. J. He, X. Zhang, X. M. Chen, Potential therapeutic effects of policosanol from insect wax on caenorhabditis elegans models of parkinson's disease. *J. Neuroimmune Pharm.* **2023**, 18, 127.

[5] a) Q. Lu, Y. Q. Bu, L. Y. Ma, R. Liu, Transgenerational reproductive and developmental toxicity of tebuconazole in caenorhabditis elegans. *J. Appl. Toxicol.* **2020**, 40, 578; b) W. X. Jiang, W. D. Yan, Q. L. Tan, Y. M. Xiao, Y. Shi, J. J. Lei, Z. Q. Li, Y. Y. Hou, T. Liu, Y. Li, The toxic differentiation of micro- and nanoplastics verified by gene-edited fluorescent caenorhabditis elegans. *Sci. Total Environ.* **2023**, 856, 159058.

[6] M. L. Tucci, A. J. Harrington, G. A. Caldwell, K. A. Caldwell,Modeling dopamine neuron degeneration in caenorhabditis elegans, G. Manfredi, H. Kawamata *Neurodegeneration: Methods and protocols*, Totowa, NJ, Humana Press, **2011**, 129.

[7] J. F. Cooper, J. M. Van Raamsdonk, Modeling parkinson's disease in *C. Elegans. J. Parkinson. Dis.* **2018**, 8, 17.

[8] X. B. Huang, C. L. Wang, T. J. Zhang, R. Z. Li, L. Chen, K. L. Leung, M. Lakso, Q. H. Zhou, H. J. Zhang, G. Wong, Piwi-interacting rna expression regulates pathogenesis in a caenorhabditis elegans model of lewy body disease. *Nat. Commun.* **2023**, 14, 6137.

[9] S. Shashikumar, H. Pradeep, S. Chinnu, P. S. Rajini, G. K. Rajanikant, Alpha-linolenic acid suppresses dopaminergic neurodegeneration induced by 6-ohda in *C. Elegans*. *Physiol. Behav.* **2015**, 151, 563.